Ion beam induced depth profile modification of fusion gases implanted in Be, C and Si.

F. Schiettekatte and G.G. Ross
INRS-Énergie et Matériaux, 1650 boul. Lionel Boulet, Varennes, Québec, J3X 1S2, Canada

A. Chevarier, N.Chevarier and A.Plantier
IPNL, Université Claude Bernard, F69622 Villeurbanne Cedex, France

ABSTRACT

A study of the depth profile modification of H, D and He implanted in beryllium, HOPG graphite, glassy carbon and silicon under 350 keV He, 2.5 MeV He and 2.54 MeV N ion beam irradiation has been conducted. Desorption rate profiles have been measured. They can be connected to the activated (detrapped) atom profiles during irradiation, according to local molecular recombination models based on the rate equations. It is found that molecular recombination between *activated* atoms stands for H and D implanted in carbon and beryllium, except for H implanted to high concentration in Be. In this case, stronger H and D trapping is observed in the vacancy profile. Also, higher desorption rate occurs near the surface of crystalline samples. Finally, it is found that the measured values of detrapping cross sections after He and N beam bombardment are in agreement with a model which assumes that the detrapping is induced by the primary recoils.

1. INTRODUCTION

It is now well established that the properties of materials can be modified by the energy deposition due to swift ions irradiation [1]. One process is the induced desorption of some atoms or molecules contained in materials. But this effect has also consequences on the quantitative aspect of Ion Beam Analysis [2] as well as on the plasma-wall interaction in Tokamak devices. Hence, many studies have been carried out on the desorption of fusion gas in materials [2-6], especially on the hydrogen isotopes in graphite.

However, it is difficult to determine how the incident ions interact with matter in order to detrap atoms. Some semi-empirical models were proposed to fit the total amount of remaining hydrogen as a function of beam fluence. They were generally based on simple or multiple exponential functions [6-9] as well as on the exponential integral [10]. Adel et al. [11-12] have proposed an equation that is based on a statistical distribution of ion impacts. Wampler and Myers [3] first proposed a physical model for carbon, including diffusion and retrapping to explain the desorption "slow down" at high fluence. All these models assume first order detrapping without in-bulk molecular recombination.

Scherzer et al. [4] added to Wampler's model a local molecular recombination term (2nd order) between activated (detrapped) atoms. According to anterior works, they assumed fast transport of these molecules to the surface. They also considered that the detrapping is induced by nuclear collisions between incident ions and trapped atoms. They calculated by means of TRIM [13]

the corresponding detrapping rate for different beam energies. However, using a set of parameters obtained by fitting a data set at a given energy, the model gave only qualitative agreement for the other energies for which the data showed faster initial desorption rate. They suggested that another detrapping mechanism induced by the incident ion primary recoils could explain the discrepancy. In their opinion, this would however multiply at the same time the number of adjustable parameters.

Tsuchiya and Morita [5] have also studied the hydrogen in graphite under MeV He irradiation. Their mass balance equations [17] assume local molecular recombination between trapped and activated atoms. By fitting an analytic solution of these equations to the desorption curves, they found the ion-induced detrapping cross section σ_d together with K/Σ_T, the ratio of the local molecular recombination constant divided by the retrapping constant. They showed that the experimental values and energy dependence of σ_d are in good agreement with theoretical prediction that assumes detrapping induced by primary C recoils.

Nevertheless, if a few experiments have been performed on hydrogen profile modification by isotopic exchange at low (keV) energies in order to explain the desorption in this energy range (see for example ref. [14]), only few works have made detailed study about the depth profile modification of implanted materials. Such study would confirm the process predicted by the models or reveal possible irregularities. So it becomes possible to highlight some phenomena as a stronger trapping in the implantation damage profile or the order of detrapping.

In this paper, we report the ion-induced depth profile modification of H, D and He implanted at low energies (keV) and various concentrations in materials of interest for fusion (beryllium, graphitic and glassy carbon) and silicon. They were submitted to 350 keV ^{4}He, 2.5 MeV ^{4}He and 2.54 MeV ^{15}N beams, covering this way different ranges of energy deposition. The compatibility with models mentioned above will be discussed.

2. DESORPTION RATE PROFILE

Given the total concentration $C(x, t) = C_t(x, t) + C_s(x, t)$ which are the concentrations of trapped and activated atoms, respectively. Let the net detrapping rate be

$$\frac{d\tilde{C}(x,t)}{dt} = \sigma_d \phi C_t(x,t) - \Sigma C_s(x,t)[\bar{C}_0 - C_t(x,t)] \tag{1}$$

where σ_d is the detrapping cross section of the incident particles, ϕ the beam flux, Σ the retrapping rate and $\bar{C}_0$ the trap density. On the one hand, for the high energy beam induced desorption, Scherzer's model [4] can be expressed by the following rate equations:

$$\begin{aligned} \frac{dC_s(x,t)}{dt} &= \frac{d\tilde{C}(x,t)}{dt} - K_{ss}C_s^2(x,t) \\ \frac{dC_t(x,t)}{dt} &= -\frac{d\tilde{C}(x,t)}{dt} \end{aligned} \tag{2}$$

where K_{ss} is the constant of molecular recombination between activated atoms. The solution of these equations with typical parameters shows that $C_s^2(x,t) \propto C(x,t)$.

On the other hand, Morita's model [5] follows the rate equations:

$$\begin{aligned} \frac{dC_s(x,t)}{dt} &= \frac{d\tilde{C}(x,t)}{dt} - K_{st}C_s(x,t)C_t(x,t) \\ \frac{dC_t(x,t)}{dt} &= -\frac{d\tilde{C}(x,t)}{dt} - K_{st}C_s(x,t)C_t(x,t) \end{aligned} \tag{3}$$

where K_{st} is the constant of molecular recombination between activated and trapped atoms. By solving eqs. (3) using typical parameters, we find that $C_s(x,t) \propto C(x,t)$. In both cases, $C_s(x,t) \ll C_t(x,t) \lesssim C(x,t)$.

Assuming a constant beam flux ϕ (with the beam fluence $\varphi=\phi t$), the *desorption* rate (not to be confused with the *detrapping* rate) can be defined as:

$$Y(x,\varphi) = -\frac{1}{C(x,\varphi)}\frac{dC(x,\varphi)}{d\varphi} = -\frac{1}{C(x,\varphi)}\left(\frac{dC_s(x,\varphi)}{d\varphi} + \frac{dC_t(x,\varphi)}{d\varphi}\right) \tag{4}$$

$Y(x,\varphi)$ gives the ratio of desorption at depth x relatively to the concentration of the depth profile $C(x,\varphi)$. It appears that for Scherzer's model,

$$Y(x,\varphi) = \frac{K_a C_s^2(x,\varphi)}{C(x,\varphi)} \sim constant \tag{5}$$

while for Morita's model

$$Y(x,\varphi) = \frac{2K_t C_s(x,\varphi)C_t(x,\varphi)}{C(x,\varphi)} \sim C(x,\varphi), \tag{6}$$

The desorption rate $Y(x,\varphi)$ can be found experimentally using two successive profiles separated by a small fluence $\Delta\varphi$:

$$Y(x,\varphi) \approx \frac{C(x,\varphi-\Delta\varphi) - C(x,\varphi)}{C(x,\varphi)\ \Delta\varphi} \tag{7}$$

In this paper, Y(x) has been calculated for many depth profiles. The raw data for $Y(x)$ are represented by symbols o with arbitrary units. The statistical error on $Y(x)$ is equal to the data point dispersion. Because the starting depth profiles are still resolution-broadened, the measured $Y(x)$ is found to be smoothed relatively to the actual curve. This kind of curve will be helpful in order to determine the uniformity (or non-uniformity) of the detrapping process, to validate models and to find if the diffusion plays a role in the desorption. Even if these models were developed for graphite, they will be used to discuss the desorption of hydrogen in beryllium for which no specific physical model is available.

3. EXPERIMENTAL

To achieve this study, a good depth resolution is necessary to get relevant depth profiles. Like most of the papers mentioned above, ERD [15] was used because it gives quantitative depth profiles and the ion-induced desorption is intrinsic to the technique. Moreover, the use of an **ExB** filter [16] (instead of an absorber foil) only limits the surface resolution to the detector resolution. Together with a beam close to the stopping power maximum, the depth resolution is optimal and sufficient for relevant observation of the depth profile modification. The 350 keV ^{4}He irradiation was also monitored by means of Multi Channel Scaling (MCS) that allows to follow more precisely the evolution of the total amount of implant during irradiation.

A description of the experimental setups used and resolution calculation can be found in ref. [18]. Briefly, the 350 keV ^{4}He analysis, were done with an incident angle of 25° relatively to the sample surface and a scattering angle of 45°. The solid angle was 2.06×10^{-5} str. The 2.5 MeV ^{4}He and 2.54 MeV ^{15}N analyses were performed with an incident angle of 15° relatively to the sample surface and a scattering angle of 30°. The solid angle was 6.6×10^{-5} str. Solid angles are small in order to minimize the spatial spread of the scattered particles and separate them properly inside the **ExB** filter. Obviously, this worsens the sensitivity as well. The depth resolution (σ) will be plotted as an horizontal error bar on some graphs. All the depth profiles (and scaling data) shown in this paper are accumulated depth profiles, i.e. they contain all the detected particles from the measurement start to the corresponding fluence. The statistical error on the first point of each scaling data set is always $\leq 10\%$.

The materials used are available commercially. The beryllium samples (Be, Beryllium Window) are polycrystalline (grain size ≈ 1 μm) with a 99.4% purity. The Highly Oriented Pyrolitic Graphite (HOPG, Union Carbide) contains 6% of hydrogen as main impurity. It has been implanted along the a-orientation. The glassy carbon (v-C, Carbone Lorraine) is amorphous and contains no measurable quantity of hydrogen. The silicon (Si) comes from a n-Si <100> wafer with the standard purity of semiconductor industry. The Be, HOPG and v-C samples were polished with a 3 μm diamond suspension followed by a 0.04 μm alumina finish. The Si samples were not polished. Nearly 100 samples were implanted with different energies and doses. The details will be given for each ion-material combination.

The ERD energy spectra were converted to depth profile by means of Alegria, a Windows 95 freeware available from the authors. Alegria is described in ref. [19]. The profiles are still resolution broadened.

4. RESULTS AND DISCUSSION

The depth profile modification is somewhat different from a material to another. The mechanisms involved in the desorption process can be very different. Therefore, the results are presented separately for each material, showing each times the H, D and He profile modification. Helium profiles were only measured by 2.54 MeV ^{15}N irradiation. It is important to note that at these energies the sputtering yields induced by He and N at an angle of 15° relatively to the surface are below 0.01 and 0.1, respectively. So it induces a negligible depth shift to the profiles.

4.1 Beryllium

a) H in Be

Be samples were implanted with hydrogen at energies of 0.8 keV and 1.5 keV and fluences ranging from $1.9 \times 10^{16} H/cm^2$ to $2.6 \times 10^{17} H/cm^2$ that correspond to peak concentrations between 0.05 and 0.62 H/Be. The H saturation concentration is near 0.3 H/Be, so some samples were oversaturated. However, the implantation damage continues to increase for these samples.

Under 2.5 MeV and 350 keV He irradiations, the hydrogen profiles are relatively stable in samples where the peak concentration does not exceed 0.12 H/Be. H desorption and depth profile modification begin to be observed above this ratio, and the desorption rate increases with the concentration. Results presented in Fig. 1 are those for the 1.5 keV implantations irradiated by the 350 keV ^{4}He beam. It appears in a) that at high He fluences, the samples implanted at 0.25 H/Be and 0.62 H/Be have a lower final retained quantity of H than the sample implanted at 0.17 H/Be and this H quantity gets even smaller than in the 0.12 H/Be sample. This is compatible with observations following laser induced desorption [21] and thermal desorption [22] where a significant decrease of the detrapping energy was seen above similar H concentration (0.15 H/Be) for all atoms. This also corresponds to the threshold where blistering starts to appear after implantation. Laser induced desorption indicated also that the desorption process is no longer limited by diffusion for those concentrations.

Fig. 1 b) shows the H depth profile modification in the 0.62 H/Be sample at He fluences corresponding to the symbols ✳ in Fig. 1 a). The desorption rate $Y(x)$ is calculated for the highest fluence profile (6.3×10^{16} He/cm^2). As it will be seen for ^{15}N irradiation, the minimum $Y(x)$ under the surface corresponds to the implantation damage profile (vacancies). If a fraction of the H atoms at this depth are trapped in vacancies instead of in interstitial sites, they are certainly bound with a higher energy. Besides, this zone could also act as a drain where the diffusing atoms or molecules from larger depths are retrapped. No retrapping is observed in depth (deeper than the profile), so no diffusion occurs in that direction.

Under ^{15}N irradiation, the hydrogen desorbes rapidly in all samples. Moreover, above the 0.15 H/Be threshold, the desorption process is much larger. Fig. 2 a) shows the evolution of the total quantity of H implanted at 0.8 keV and fluences between $1.9x10^{16}H/cm^2$ and $1.5x10^{17}H/cm^2$ that correspond to peak concentrations ranging from 0.05 to 0.40 H/Be. In this graph, the solid symbols represent the implanted dose of H, also confirmed by 2.5 MeV ^4He beam measurement. However, for the sample implanted to 0.40 H/Be, the solid symbol corresponds to the *retained* H quantity measured by 2.5 MeV ^4He beam. It is seen that the H concentration in the 0.05 H/Be sample rapidly reaches a plateau (7.5×10^{15} H/cm^2), while in the 0.15 H/Be sample, H concentration still decreases at higher N fluences. It is impressive to see that the 0.25 H/Be and 0.40 H/Be samples have lost nearly 50% of their hydrogen after irradiation of only 6×10^{13} N/cm^2. Moreover, the final H quantity of both samples are much lower than that in the 0.15 H/Be sample. For 0.25 and 0.40 H/Be samples, both curves superimpose (similar initial retained H concentration) so it seems that their is no effect due to the increase of implantation damage.

Fig. 2b) shows the H depth profile evolution in the 0.15 H/Be sample. It is seen that at high ^{15}N fluences, the desorption rate $Y(x)$ is almost constant on all the depth range except for the rise near the surface. This effect was not observed after 350 keV ^4He beam irradiation because of the relative H stability.

Above this concentration (0.15 H/Be), we observe the same type of H profile modification as seen under 350 keV ^4He irradiation. The H depth profile modification in the 0.40 H/Be sample is shown in Fig 2c). The highest fluence profile is also plotted in Fig. 2d) together with the vacancy

profile (calculated by means of TRIM-95 [13]). Once more, a minimum in the desorption rate is seen just under the surface. Moreover, the vacancy profile exactly matches with the peak in H depth profile. At this time, a maximum arises in the desorption rate profile. No in-depth diffusion is observed.

Thus, the beam induced detrapping of hydrogen implanted in Be follows two different regimes depending of the initial H concentration. At H peak concentration ≤ 0.12 H/Be, H is more firmly bound. The desorption rate profile could be compatible with Scherzer's model, although laser desorption experiments showed that diffusion plays a significant role below 0.15 H/Be [23]. Above this critical concentration, the desorption rate profile starts to follow the shape of the profile, except in the damaged zone where the trapped particles are bound with higher energy. This effect was not observed under the critical H concentration. In that regime, the desorption rate complies with Morita's model. Because no in-depth diffusion is observed, the unimplanted, unirradiated Be seems to acts as a diffusion barrier.

b) D in Be

1.6 keV D with fluences ranging from 1.0×10^{16}D/cm^2 to 2.5×10^{17}D/cm^2 was implanted in Be and analyzed by means of 350 keV ^{4}He and 2.54 MeV ^{15}N beams. As seen in Fig. 3a), although their is no D desorption under He irradiation in samples with D peak concentrations ≤0.15 D/Be, the desorption rate of the sample implanted to 0.30 D/Be is slower than for H. In Fig. 3b), the D profile evolution of the 0.30 D/Be sample following He irradiation shows almost the same shape of

desorption rate observed for the H (Fig. 1b). Thus, even if the D desorbes more slowly, the same transition is observed.

c) He in Be

Helium was implanted in Be at energies of 0.8 keV, 1.5 keV, 5 keV and 10 keV with fluences ranging from 4.7×10^{15}He/cm^2 to 1.0×10^{17}He/cm^2 . Helium was profiled by 2.54 MeV ^{15}N beam. In spite of the high energy deposition, only small He desorption is observed (<5%). This is consistent with the observations of P. Jung [20] who found only small thermal desorption of the implanted helium even at a temperature close to the melting point. Obviously, helium atoms are detrapped in a first order process. Two possibilities come out: 1) the trapped helium is bound with an energy high enough to prevent any detrapping, 2) its diffusion coefficient is so low that it is retrapped before it has time to move in the lattice. A heavier beam (with higher energy deposition) could be used in order to determine if He atoms are finally detrapped and desorbed or if the diffusion process still limits its desorption.

4.2 Highly Oriented Pyrolitic Graphite (HOPG)

a) H in HOPG

HOPG graphite was H implanted with energies of 0.8 keV and 1.5 keV and fluences ranging from 1.0×10^{16}H/cm^2 to 1.3×10^{17}H/cm^2 that correspond to peak concentrations ranging from 0.05 to

0.35 H/C. Thus, the saturation of 0.4 H/C was not reached or exceeded. It is worth mentionning that HOPG has already a 0.06 H/C background that also desorbes.

In these experiments, He beam induced desorption is observed for all concentrations as shown in Fig. 4a) for the 1.5 keV H implantations. In these measurements, the H background represents $5x10^{16}$ H/cm^2 of the initial concentration. It is seen in Fig. 4a) from a He fluence to the other, there is a similar difference in the retained quantity of H, except for the 0.30 H/C sample at low beam fluence. This could be explained if one assumes that: 1) the 6% H background is responsible for the most part of the initial decrease in the 0.05, 0.10 and 0.25 H/C samples so very similar absolute H quantity was released from these samples during the first $3x10^{16}$ He/cm^2 irradiation; 2) the H background was desorbed from the 0.30 H/C sample during the implantation because it was implanted close to saturation, so no such H background desorption is observed at low He beam fluence. Hence, the implanted H desorbes more slowly than the H background. Besides, at high fluence, the implanted H desorption increases gradually with the concentration, but the total H quantity in a sample never falls under the quantity of another sample implanted at lower concentration, as seen in beryllium above 0.15 H/Be.

Fig. 4 shows also H depth profile modification for a low (b) and high (c) H/C concentrations. H desorption occurs preferentially near the surface. In Fig. 4b), the H desorption rate from the 0.10 H/C sample, following a high 350 keV ^{4}He fluence, decreases continuously from the surface until a depth of $4x10^{17}$ C/cm^2. This decrease will be called "surface ramp". In Fig. 4c) the same feature is observed at the same rate in the 0.30 H/C sample. However, the surface ramp is overcome by a

constant desorption rate. The value of this constant desorption rate augments with the H concentration and complies with Scherzer's model (also plotted in Fig. 4c). The surface ramp points out that a diffusion process probably occurs so that the hydrogen closer to the surface is more easily desorbed. This process is not influenced by the sample H concentration. Identical surface ramp is observed for the lower energy implantation (0.8 keV) but it covers the entire range of implantation. Hence, the surface ramp seems to have a constant maximum depth. Similar diffusion and retrapping process could be responsible for the $Y(x)$ decrease at the end of both profiles (~7×10^{17} C/cm^2).

As expected, Fig. 5 shows that under ^{15}N bombardment the H desorption is much faster. Only 0.8 keV H implanted samples were depth profiled. Fig. 5a) shows the evolution of the total H quantity as a function of N fluence. Solid symbols represent the H dose as measured by means of low fluence 2.5 MeV ^{4}He beam. Once again, a part of the total dose (~6×10^{16}H/cm^2) comes from the 0.06 H/C background that also desorbes. As seen for H in Be, very high initial H desorption occurs below 6×10^{13} N/cm^2 for the higher H concentration samples. It is seen that ~60% of the H is desorbed in the first 6×10^{13} N/cm^2 irradiation. However, at a given N fluence, the total H quantity of a sample is always higher than the quantity of another sample implanted at lower concentration, as observed under 350 keV ^{4}He irradiation.

Fig. 5 b) shows the H depth profile modification in the 0.35 H/C sample together with the desorption rate (Fig. 5c). This desorption rate induced by a high N fluence features a surface ramp that extends far in depth to 10^{18} C/cm^2. Hence, it seems that the beam species influences the maximum depth of the surface ramp. Also, no constant detrapping rate is observed as seen for similar implanted

concentration after 350 keV ^{4}He irradiation (Fig. 4c). However, the desorption rate was calculated after a high fluence N bombardment, so the H concentration of the profiles is very low (~2%). Hence, this case is more similar to Fig 4b). In both cases, the net detrapping rate (eq. 1) is low because the number of available traps is high. The desorption of activated atoms vanishes accordingly, while the process corresponding to the surface ramp is still active.

To sum up, the mechanism for H desorption in HOPG can be modeled in part by the Scherzer's equations. However, this model does not explain the surface ramp for which diffusion to the surface is more likely to be the driving force. Contrary to H in Be, no preferential trapping is observed in the implantation damage profile (which is low for graphite). In the H concentration range covered in our experiment, the desorption simply increases with concentration without any particular irregularity due to H concentration. At low concentrations (H/C<0.15), the desorption process is somewhat faster than for H in Be (H/Be<0.15). The H desorption from the 0.06 H/C background is faster than the desorption of the implanted H, but this is not sufficient to account for the very high desorption at very low N fluence, at least in the HOPG samples implanted to high H concentrations.

b) D in HOPG

Because the ERD sensitivity is much lower for deuterium (cross section is lower), the D depth profile modification is more difficult to analyze. Nevertheless, if moderated H desorption was observed under 350 keV ^{4}He irradiation, only very low desorption occurs for D. D desorption

induced by 2.54 MeV ^{15}N irradiation is also lower than for H. D implanted in a HOPG sample to a low concentration was profiled by means of N beam. 82% of the D was retained after a fluence of $1.5x10^{15}$ N/cm^2 while less than 60% of the implanted H was retained in the 0.05 H/C sample (Fig. 5a). Once more, an important isotopic effect is observed in the trapping energy and/or detrapping probability. However, the desorption process is similar for H and D. The desorption rate is constant all over the depth profile, in agreement with Scherzer's model. As observed for H, preferential D desorption occurs near the surface.

c) He in HOPG

Helium is not retained in HOPG when implanted at low energy. Only He implanted at 10 keV was retained (25%). Helium is necessarily detrapped in a first order process. However, the evolution of the total He quantity following N irradiation does not correspond to an exponential. Fig. 6 shows the He depth profile modification after 2.54 MeV ^{15}N irradiation. As observed for H, preferential desorption occurs closer to the surface. In bulk, the desorption rate decreases with depth as seen for H in HOPG. However, the desorption rate becomes very high in the first 2×10^{17} C/cm^2 depth. Hence, diffusion gets higher close to the surface. This could be explained by the crystallinity of the HOPG if it is taken into account that He is trapped in the crystal defects. Therefore, desorption of He in HOPG follows similar desorption mechanism than H at low concentration.

4.3 Hydrogen in Glassy carbon (v-C)

Contrary to the HOPG that has a highly oriented polycrystalline structure, v-C has an uniform amorphous structure. It was observed that H implanted to peak concentration of 0.10 H/C is stable under 350 keV ^{4}He irradiation. However the 0.40 H/C sample undergoes a high decrease in its H contents (50% after 4.2×10^{16} He/cm^2 irradiation). Fig. 7 shows the H profile modification for this sample. At high He fluence, it appears that the desorption rate is uniform all over the depth profile except for a decrease (and some retrapping) deeper that 6×10^{17} C/cm^2. Except for that feature, which could be due to diffusion, the desorption process is compatible with Scherzer's model. The H detrapping rate profile does not show a surface ramp as observed in the HOPG. This could indicate that the surface ramp was due to enhanced diffusion close to the surface because of the local cristalinity of the HOPG near the surface.

4.4 H and He in Silicon

A few Si samples were implanted with 0.8 keV H and 1.6 keV He at normal incidence (with a possibility of low energy channeling [24]) to fluences ranging from $1.7\text{x}10^{16}$H/cm^2 to $7.5\text{x}10^{16}$H/cm^2 and from $2.4\text{x}10^{15}$He/cm^2 to $1.0\text{x}10^{16}$He/cm^2, respectively. As observed in previous works [2], no H desorption occurs under 350 keV ^{4}He irradiation. H and He depth profiles were also obtained by mean of 2.54 MeV ^{15}N beam. Fig. 8a) shows the evolution of the total H and He quantity after different N fluences. Solid symbols represent the implanted doses. The desorption rates are

moderated or low, except for the 0.15 H/Si sample. Its depth profile is plotted in Fig. 8b) for different N fluences. An important surface peak is present at low N fluence and vanishes rapidly. This could be due to surface water vapour adsorption but no such peak was observed with 2.5 MeV ^{4}He beam. Also, LN_2 cold trap was used during the experiment that usually avoids water contamination. Another possible explanation is that the H has a high surface binding energy on Si relatively to Be and C so the detrapped and diffusing H still adsorbed on Si surface during initial (high rate) detrapping. Because H in Si is stable under He irradiation, it would not have been observed.

5. DETRAPPING CROSS SECTION

Figs. 4c) and 7) show that Scherzer's model [4] complies with the H desorption rate profile observed in carbon. However, the authors assumed that H detrapping occurs through nuclear collisions between incident ions and trapped atoms. According to the authors themselves and as mentioned in introduction, this detrapping mechanism is no sufficient to explain the early desorption rate. Tsuchiya and Morita have considered the hydrogen detrapping induced by primary recoils and developed a theoretical expression for the detrapping cross section σ_d [5]. This equation predicts a lower desorption rate for D compared to H and states that,

$$\sigma_d \propto Z_{beam}^2 M_{beam} \approx \frac{dE}{dx} \qquad (8)$$

They implanted H to saturation in graphite and measured σ_d after He irradiation of energies ranging from 800 keV to 1.9 MeV. They found a good agreement between their experimental and

theoretical values. For saturated samples, the detrapping cross section can be found from the early desorption rate (at very low beam fluence), because the retrapping process (right hand side of eq. 1) is small in saturation conditions. For H implanted to saturation in HOPG, our σ_d values are also in relatively good agreement with Tsuchiya and Morita equation. We found $\sigma_d = 2.5\text{x}10^{-17}$ with the 2.5 MeV ^{4}He beam and $\sigma_d = 9.2\text{x}10^{-16}$ with the 2.54 MeV ^{15}N beam. The ratio of 37 between these two values is somewhat in good agreement with the a ratio of 46 predicted by eq. (8). Moreover, we found that the D detrapping rates were lower than the H ones, as predicted by the Tsuchiya and Morita equation.

6. CONCLUSION

A study of the depth profile modification of H, D and He implanted in materials under high energy ion beam irradiation has been presented. The good depth resolution of the ERD-ExB technique has allowed to measure for the first time the desorption rate, which can be connected to the activated (detrapped) atom profiles according to Scherzer's and Morita's physical models. Table 1 gives a summary of the results. The effect of the different beam species and energies on the total amount can be assessed. It is clearly seen that the decrease of the implant concentration is relatively higher for samples implanted to high concentrations compared to those implanted to low concentration (except for the HOPG implanted with H). In the HOPG samples, the effect is equivalent or even stronger for low H concentrations. This is due to the H background that desorbes more rapidly than the implanted H. Because it contributes for a larger proportion to the total amount

in the low concentration samples, the H desorption appears to be stronger. However, if the effect of the H background is subtracted, the H desorption is found to be higher for HOPG samples implanted to high H concentration. Table 1 also shows that an isotopic effect is observed in all samples when H and D desorptions are compared. D desorption is always much lower.

The desorption rates of H and D in carbon at high beam fluences validate Scherzer's model who assumes recombination between activated atoms. It does not explain the enhanced desorption surface ramp observed in HOPG. This ramp, which was not seen in glassy carbon, was probably due to the HOPG cristalinity. The desorption of H implanted at low concentration in Be (<0.12 H/Be) also complies with Scherzer's model. However, at high H concentrations, the desorption rate is minimum in the vacancy profile region while deeper it follows the profile shape. Therefore, it complies with Morita's model in the deeper region. The transition in the H desorption level seen above 0.12 H/Be was also observed by laser induced desorption [21] and thermal desorption [22]. It corresponds to the threshold where blistering starts to be observed after the implantation.

The detrapping cross sections of the He and N beams are in agreement with Tsuchiya and Morita equation which assumes that the desorption is induced by the primary recoils. The N beam was used to see the effect of a higher energy deposition on depth profile modification. The high H desorption rates measured suggest to be very careful when using some Nuclear Resonance Reaction Analysis (NRRA) for the high resolution profiling of hydrogen (e.g.: $p(^{15}N,\alpha)^{12}C$ at 6.385 MeV [25]).

ACKNOWLEDGEMENT

The authors want to thank Mr Jacques Pelletier and Mr Alain Gardon for excellent accelerator operation. This work has been supported by the Natural Sciences and Engineering Research Council of Canada and by a France-Québec collaboration.

REFERENCES

[1] J. Davenas, A. Dunlop, F. Rullier-Albenque, C. Jaouen and C. Templier, Materials under irradiation, Solid State Phenomena, vol. 30-31 (Trans Tech, 1993)

[2] G.G. Ross and I. Richard, Nucl. Instr and Meth. B64 (1992) 603

[3] W.R. Wampler and S. M. Myers, J.Nucl.Mater. 111-112 (1982) 616

[4] B.M.U. Sherzer, W. Wielunski, W. Möller, A. Turos and J. Roth, Nucl. Instr and Meth. B33 (1988) 714

[5] B. Tsuchiya and K. Morita, J. Nucl. Sci. Technol. 31 (1994) 1301

[6] J. Roth, B.M.U. Scherzer, R.S. Blewer, D.K. Brice, S.T. Picraux and W.R. Wampler, J. Nucl. Mater 93-94 (1980) 601

[7] J.P. Bugeat and E. Liegeon, Nucl. Instr. and Meth. 159 (1979) 117.

[8] B.M.U. Sherzer, R.S. Blewer, R. Behrisch, R. Schulz, J. Roth, J. Borders and R. Langley, J. Nucl. Mater. 85-86 (1979) 1025.

[9] H. Baumann, T. Rupp, K. Bethge, P. Koild and C. Wild, European Mater. Res. Soc. Conf. Proc. 17 (1987) 343

[10] S. Turgeon and R.W. Paynter, Nucl. Instr. and Meth. B118 (1996) 322

[11] F. Abel, V. Quillet and M. Schott, Nucl. Instr and Meth. B105 (1995) 86

[12] M.E. Adel, O. Amir, R. Kalish and L.C. Feldman, J. Appl. Phys 66 (1989) 3248

[13] J.F. Ziegler and J.P.Biersack, The Stopping and Range of Ions in Solids, Pergamon Press, New York (1985)

[14] S. Nagata, S. Yamaguchi, H. Bergsåker and B.Emmoth, Nucl. Instr. and Meth. B33 (1988) 739

[15] J. L'Écuyer et al. J.Appl.Phys. 47 (1976) 381

[16] G.G. Ross and L.Leblanc, Nucl. Instr. and Methods B83 (1993) 15

[17] K. Morita and Y. Hasebe, J. Nucl. Mater. 176-177 (1990) 213

[18] F. Schiettekatte, A. Chevarier, N.Chevarier, A.Plantier and G.G. Ross. Nucl. Instr. and Meth. B118 (1996) 307

[19] F. Schiettekatte and G.G. Ross. "ERD spectrum to depth profile conversion program for Windows". Accepted for publication in the Proceeding of the 14th International Conference on the Application of Accelerators in Research and Industry, AIP Press, 1996

[20] P. Jung, J. Nucl. Mater. 202 (1993) 210.

[21] F. Schiettekatte, D. Kéroack, G.G. Ross and B. Terreault. Nucl. Instr. and Meth. B90 (1994) 401

[22] W.R. Wampler, J. Nucl. Mater. 122 (1984) 1598

[23] Papier de Daniel~~e~~ montrant qu'il y a de la diffusion pour D/Be<0.15

[24] Papier de Gilles sur canalisation

[25] W.A. Landford, H.P. Trautvetter, J.F. Ziegler and J. Keller, Appl. Phys. Lett. 28 (1976) 566

Table 1. Summary table: % of implant retained after low and high beam fluences. The values for the lowest and highest implanted concentration are shown (generally around 5 at% and ~35 at%, respectively). The relevant physical model also appears (S=Scherzer, M=Morita).

Mater.	Beam (keV)	Implant	retained after 10^{14} at/cm^2 (lower/higher concentration)	retained after 1.5×10^{16} at/cm^2 (lower/higher concentration)	Model
Be	^{4}He (350)	H	100% / 100%	>90% / 60%	?/M
		D	100% / 100%	100% / 88%	?/M
	^{4}He (2500)	H	n.a. / 100%	n.a. / 74%	n.a./S
	^{15}N (2540)	H	100% / 55%	50% / 17%	S/M
		^{4}He	n.a. / 100%	n.a. / >90%	-
v-C	^{4}He (350)	H	100% / 100%	>90% / 76%	?/S
HOPG		H	100% / 100%	67% / 76%	S*/S
		D	100% / 100%	100% / >90%	?
	^{4}He (2500)	H	100% / 100%	57% / 70%	S/S
	^{15}N (2540)	H	54% / 34%	8% / 10%	S*/S*
		D	100% / n.a.	82% / n.a.	S/n.a.
		^{4}He	25% after implantation	80% (of initial 25%)	-
Si	^{4}He (350)	H	100% / 100%	100% / 100%	?
		D	100% / 100%	100% / 100%	?
	^{15}N (2540)	H	100% / 100%	48% / 57%	-
		^{4}He	100% / 100%	86% / 68%	-

? : not enough desorption to calculate relevant desorption rate profile

* : no constant desorption rate was actually observed (Scherzer's model) due to the low concentration even if related results support it.

FIGURE CAPTION

Fig. 1 1.6 keV H implanted in Be after 350 keV ^{4}He irradiation a) Multi-Channel Scaling data (symbols ✳ represent the H quantity found in (b). b) H depth profile modification for the 0.62 H/Be sample. The desorption rate as a function of depth (– ⊖ –) after a fluence of (6.3×10^{16} He/cm^2) also apears.

Fig. 2 0.8 keV H implanted in Be after 2.54 MeV ^{15}N irradiation. a) Evolution of H quantity. b) H depth profile evolution in the 0.15 H/Be sample. c) H depth profile evolution in the 0.40 H/Be sample. The last fluence profile appears also in d) together with the vacancy profile. In both b) and d), symbols – ⊖ – are the desorption rate.

Fig. 3 1.6 keV D implanted in Be after 350 keV ^{4}He irradiation a) Multi-Channel Scaling data (symbols ✳ represent the H quantity found in (b). b) D depth profile modification for the 0.30 D/Be sample. The desorption rate (– ⊖ –) after a fluence of (9.4×10^{16} He/cm^2) also apears.

Fig. 4 1.5 keV H implanted in HOPG after 350 keV ^{4}He irradiation. a) Multi-Cannel Scalling data. Symbols ● represent the implanted concentration including H background while symbols ✳ are the H quantity found in (b) and (c). b) H depth profile modification for the 0.10 H/C sample. The desorption rates data (– ⊖ –) after a fluence of 7.5×10^{16} He/cm^2 is also shown. c) H depth profile modification for the 0.30 H/C samples. Also appear the desorption rate data (O) after a fluence of 3.0×10^{16} He/cm^2 and calculated according to Scherzer's model (– · · –).

Fig. 5 0.8 keV H implanted in HOPG after 2.54 MeV ^{15}N irradiation. a) Evolution of H quantity; the inset is the same graph plotted with a logarithmic fluence scale. b) H depth profile evolution in the 0.35 H/C sample. c) Desorption rate data (– ⊖ –) for the highest N fluence profile.

Fig. 6 Depth profile modification of 10 keV He implanted in HOPG to fluence of 1×10^{17}He/cm^2 after N irradiation. The desorption rate data (– ⊖ –) also apears.

Fig. 7 Depth profile modification of 1.5 keV H implanted in v-C to a fluence of 1.7×10^{17} H/cm^2 after N irradiation. Also apear the desorption rate data (O) and calculated according to Scherzer's model (– · · –).

Fig. 8 0.8 keV H and 1.6 keV He implanted in Si after 2.54 MeV ^{15}N irradiation. a) Evolution of the total H or He quantity. b) H depth profile evolution in the 0.15 H/Si sample together with the desorption rate (– ⊖ –).

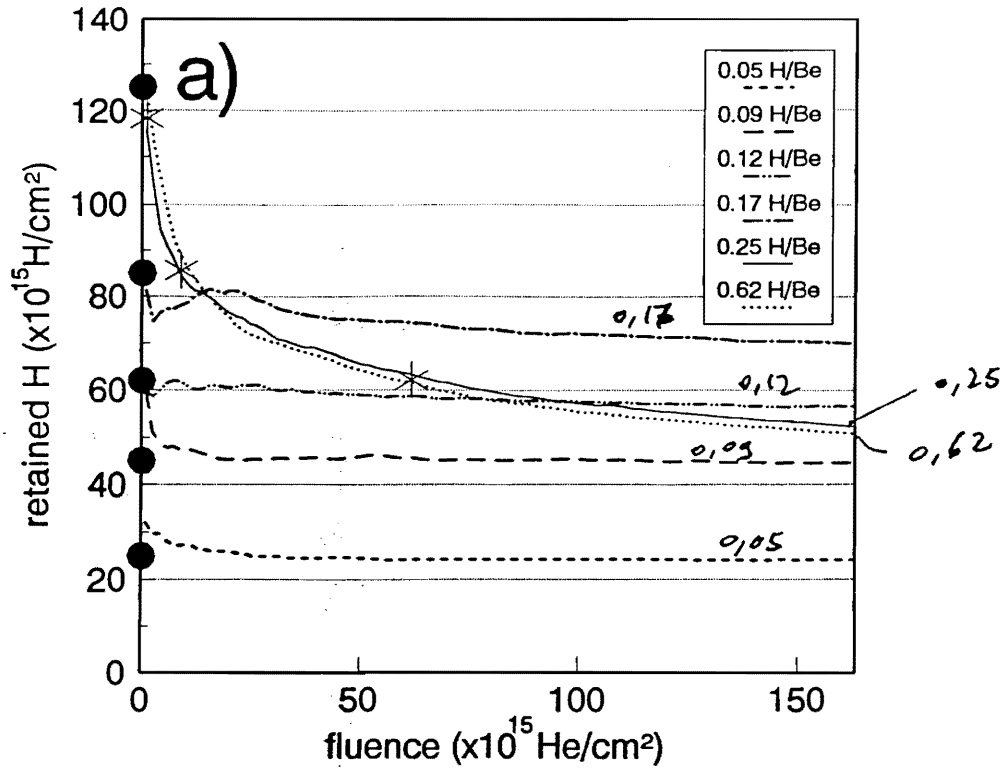
a)
0.05 H/Be
0.09 H/Be
0.12 H/Be
0.17 H/Be
0.25 H/Be
0.62 H/Be
0,17
0,12
0,25
0,62
0,09
0,05
retained H (x10^15 H/cm²)
fluence (x10^15 He/cm²)
0
20
40
60
80
100
120
140
0
50
100
150

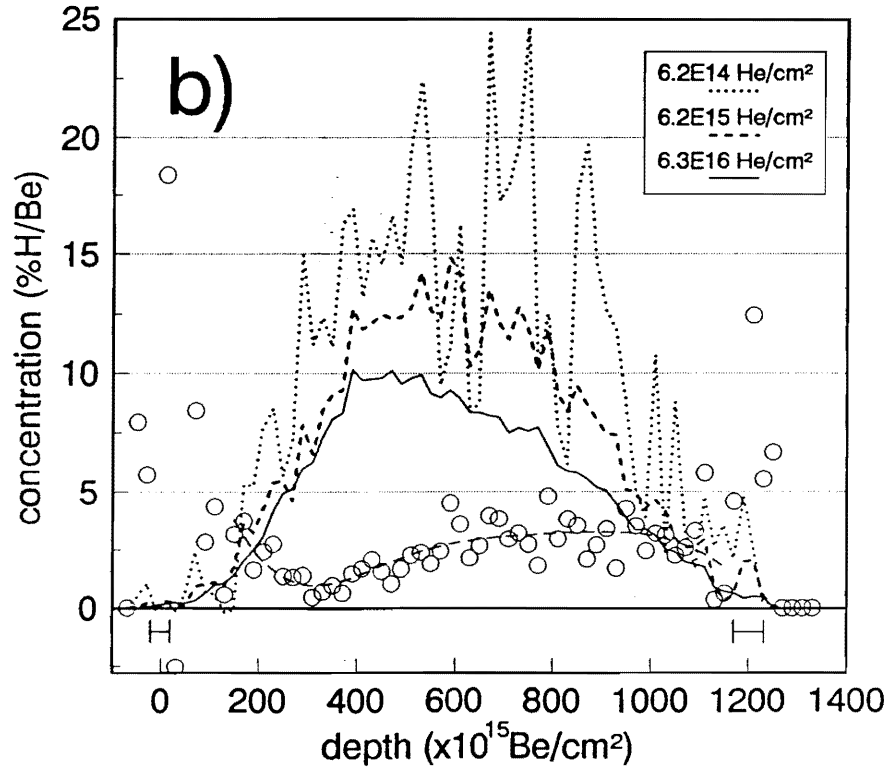
b)
6.2E14 He/cm²
6.2E15 He/cm²
6.3E16 He/cm²
concentration (%H/Be)
depth (x10^15 Be/cm²)
0
5
10
15
20
25
0
200
400
600
800
1000
1200
1400

Figure 1

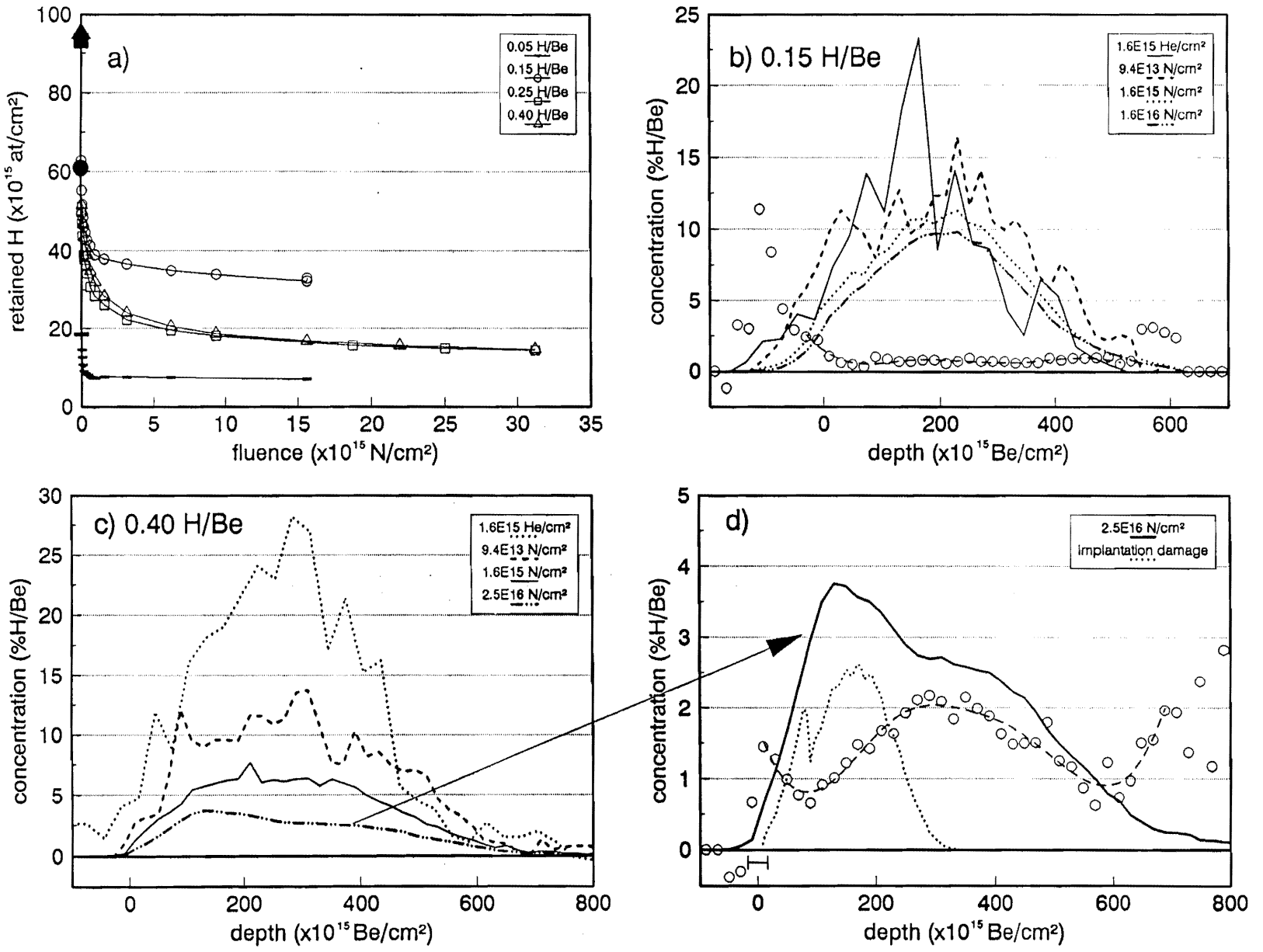
a)
0.05 H/Be
0.15 H/Be
0.25 H/Be
0.40 H/Be
retained H (x10^15 at/cm²)
fluence (x10^15 N/cm²)
b) 0.15 H/Be
1.6E15 He/cm²
9.4E13 N/cm²
1.6E15 N/cm²
1.6E16 N/cm²
concentration (%H/Be)
depth (x10^15 Be/cm²)
c) 0.40 H/Be
1.6E15 He/cm²
9.4E13 N/cm²
1.6E15 N/cm²
2.5E16 N/cm²
concentration (%H/Be)
depth (x10^15 Be/cm²)
d)
2.5E16 N/cm²
implantation damage
concentration (%H/Be)
depth (x10^15 Be/cm²)

Figure 2

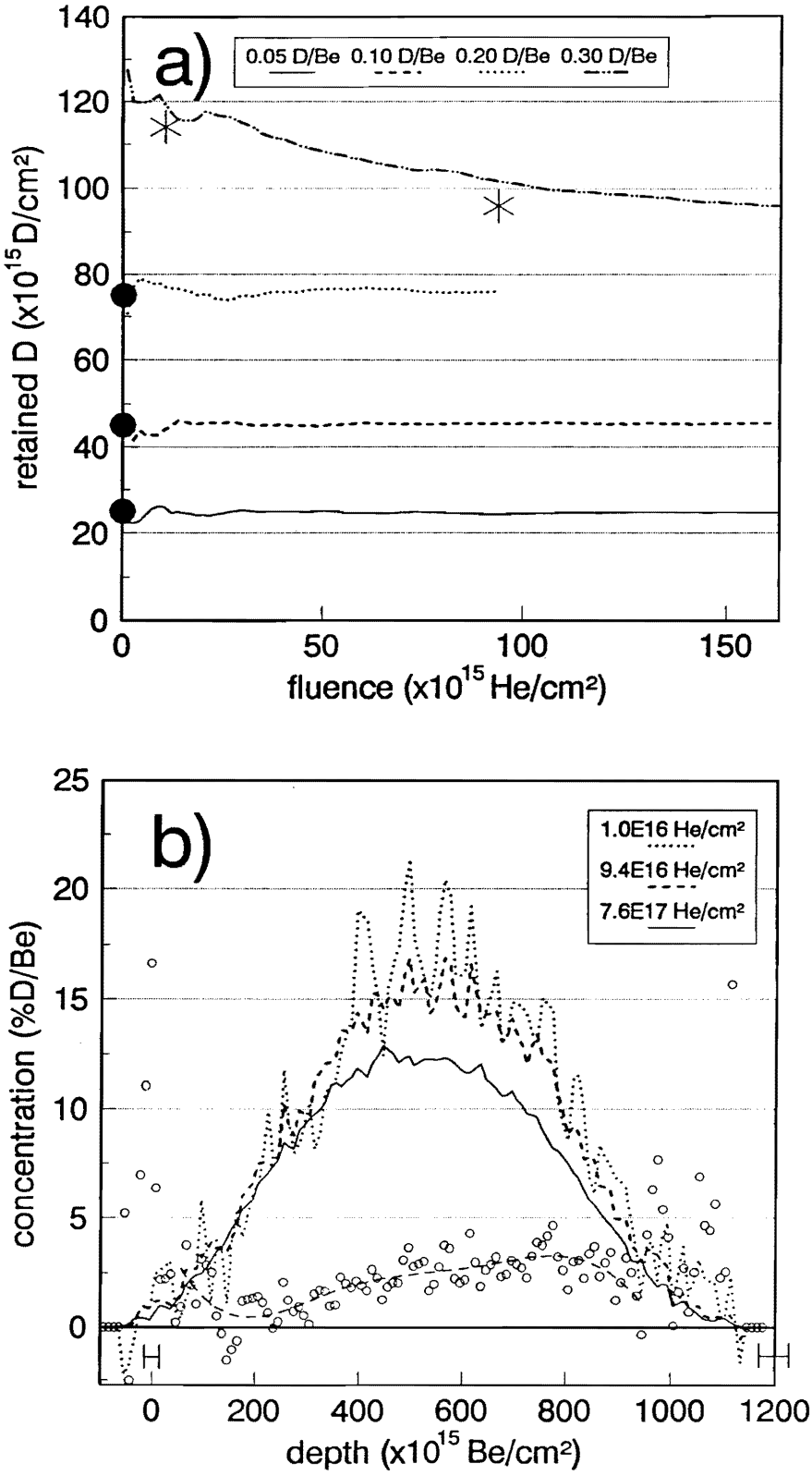
a)
0.05 D/Be
0.10 D/Be
0.20 D/Be
0.30 D/Be
retained D (x10^15 D/cm²)
fluence (x10^15 He/cm²)
0
20
40
60
80
100
120
140
0
50
100
150
b)
1.0E16 He/cm²
9.4E16 He/cm²
7.6E17 He/cm²
concentration (%D/Be)
depth (x10^15 Be/cm²)
0
5
10
15
20
25
0
200
400
600
800
1000
1200

Figure 3

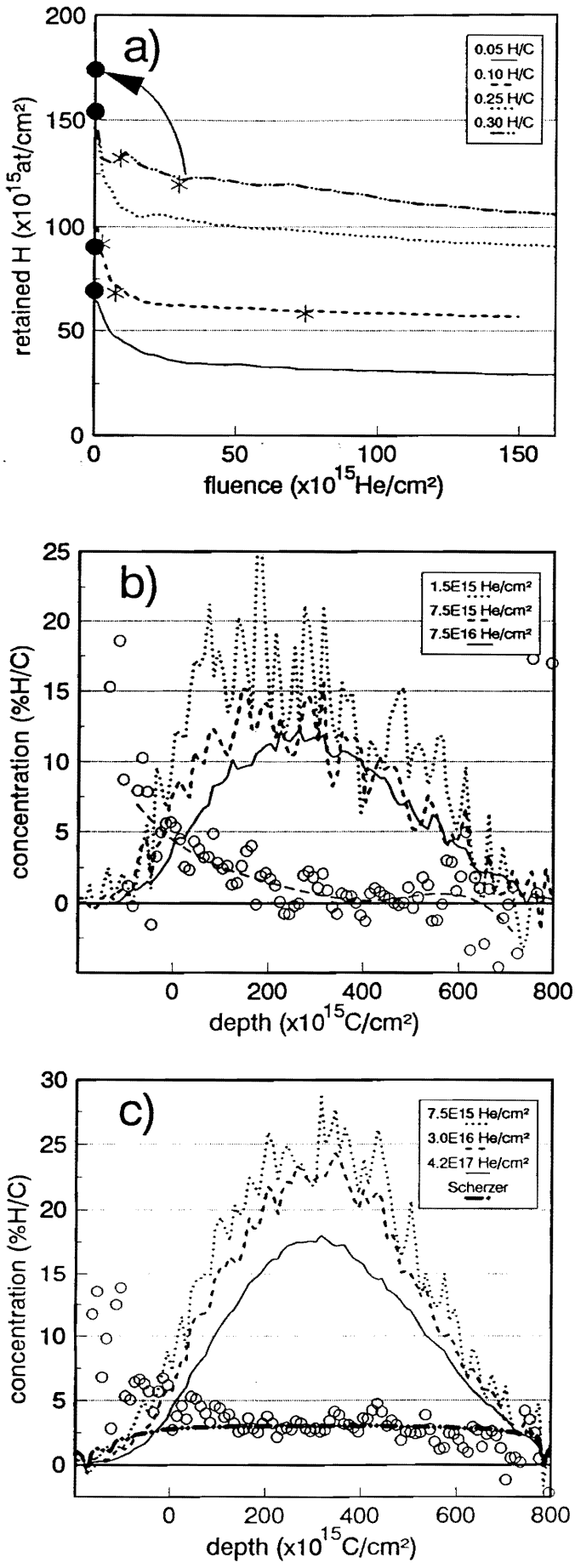
a)
0.05 H/C
0.10 H/C
0.25 H/C
0.30 H/C
retained H (x10^15 at/cm²)
fluence (x10^15 He/cm²)
b)
1.5E15 He/cm²
7.5E15 He/cm²
7.5E16 He/cm²
concentration (%H/C)
depth (x10^15 C/cm²)
c)
7.5E15 He/cm²
3.0E16 He/cm²
4.2E17 He/cm²
Scherzer
concentration (%H/C)
depth (x10^15 C/cm²)

Figure 4

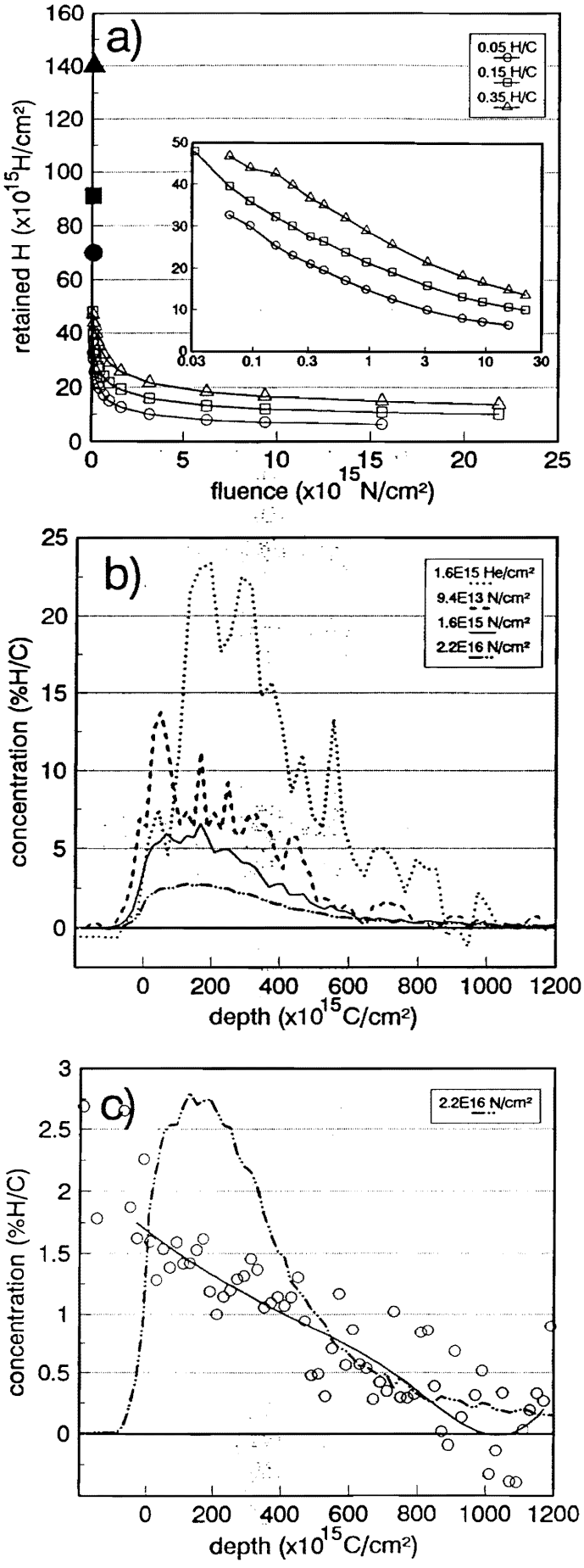
a)
0.05 H/C
0.15 H/C
0.35 H/C
retained H (x10^15 H/cm²)
fluence (x10^15 N/cm²)
b)
1.6E15 He/cm²
9.4E13 N/cm²
1.6E15 N/cm²
2.2E16 N/cm²
concentration (%H/C)
depth (x10^15 C/cm²)
c)
2.2E16 N/cm²
concentration (%H/C)
depth (x10^15 C/cm²)

Figure 5

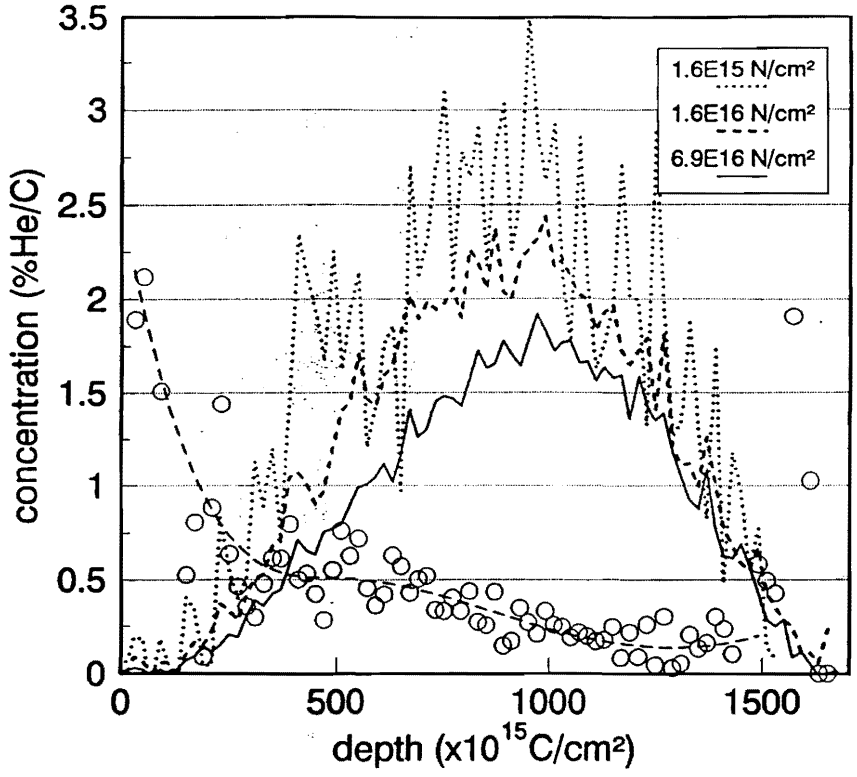
3.5
3
2.5
2
1.5
1
0.5
0
concentration (%He/C)
0
500
1000
1500
depth (x10^{15}C/cm²)
1.6E15 N/cm²
1.6E16 N/cm²
6.9E16 N/cm²

Figure 6

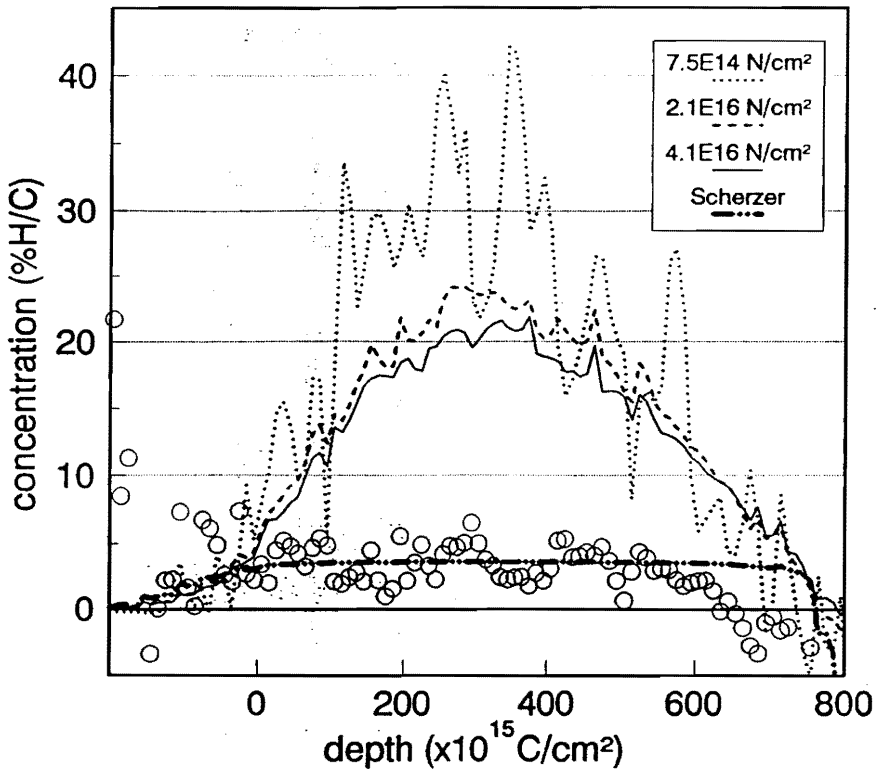
7.5E14 N/cm²
2.1E16 N/cm²
4.1E16 N/cm²
Scherzer
concentration (%H/C)
40
30
20
10
0
0
200
400
600
800
depth (x10^15 C/cm²)

Figure 7

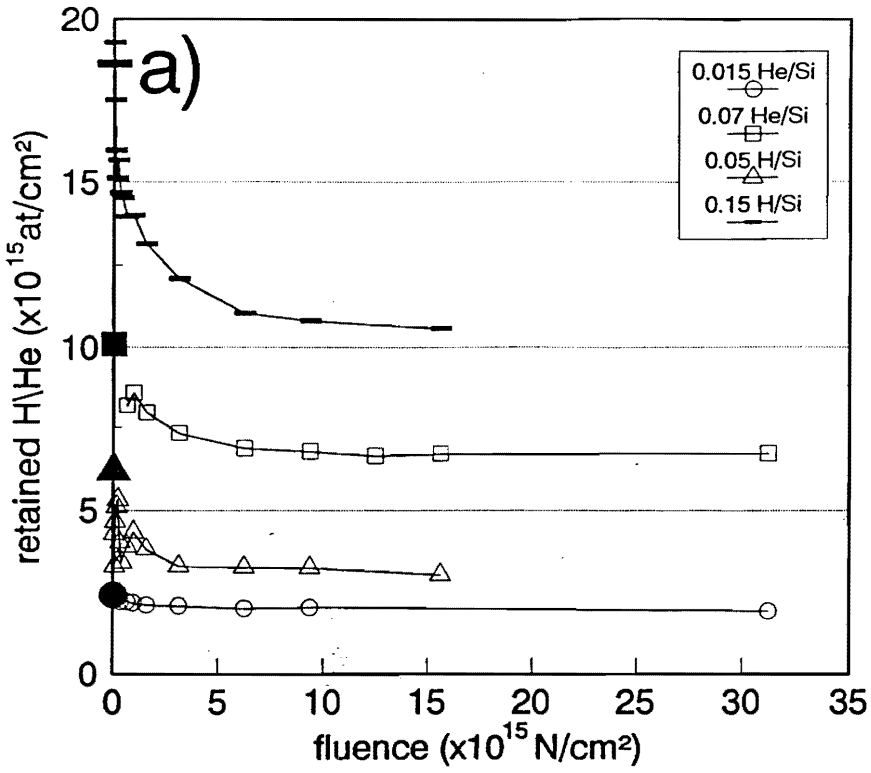
a)
0.015 He/Si
0.07 He/Si
0.05 H/Si
0.15 H/Si
retained H\He (x10^15 at/cm²)
fluence (x10^15 N/cm²)
0
5
10
15
20
25
30
35

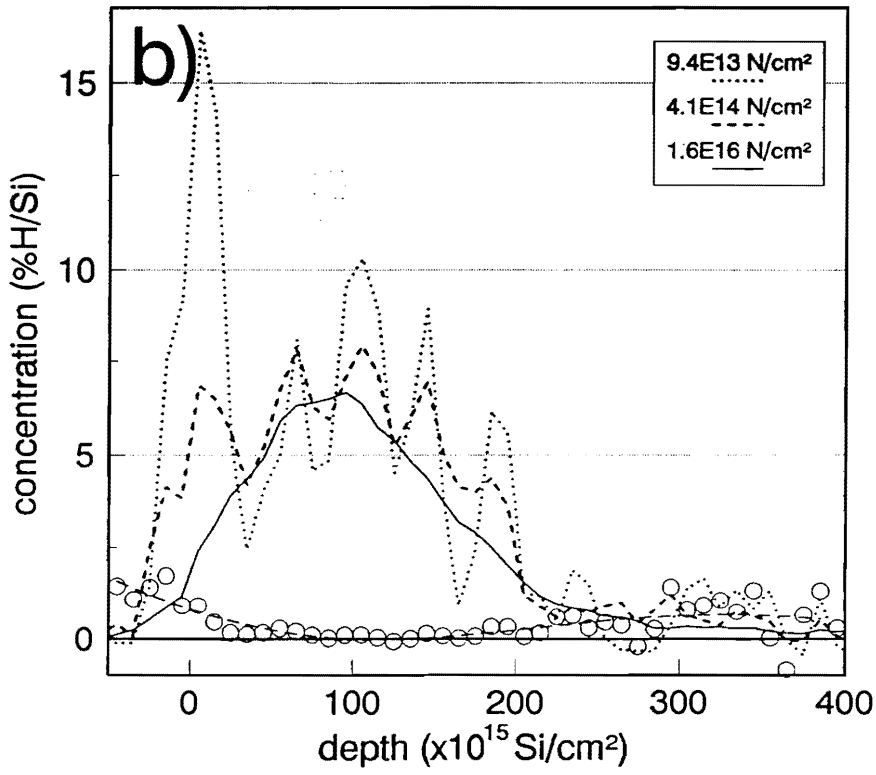
b)
9.4E13 N/cm²
4.1E14 N/cm²
1.6E16 N/cm²
concentration (%H/Si)
depth (x10^15 Si/cm²)
0
100
200
300
400

Figure 8